

Effect of Molecular Orientation on Mechanical Property of Single Electrospun Fiber of Poly[(R)-3-hydroxybutyrate-*co*-(R)-3-hydroxyvalerate]

Kok Ho Kent Chan,[†] Siew Yee Wong,[‡] Xu Li,^{*,‡} Yan Zhong Zhang,[§] Poh Chong Lim,[‡] Chwee Teck Lim,[§] Masaya Kotaki,^{*,†} and Chao Bin He^{*,‡}

*Advanced Fibro Science, Kyoto Institute of Technology, Matsugasaki, Sakyo-Ku, Kyoto 606-8585, Japan, Institute of Materials Research and Engineering, A*STAR (Agency for Science, Technology and Research), 3 Research Link, Singapore 117602, Singapore, and Division of Bioengineering, Faculty of Engineering, National University of Singapore, 9 Engineering Drive 1, Singapore 117576, Singapore*

Received: June 21, 2009; Revised Manuscript Received: August 25, 2009

Electrospun poly[(R)-3-hydroxybutyrate-*co*-(R)-3-hydroxyvalerate] (PHBV) fibers were collected by using a counter electrode collector or a rotating disk collector. The molecular orientation and mechanical property of single PHBV fiber were studied. 2-D wide-angle X-ray diffraction and polarized Fourier transform infrared spectra of the macroscopically aligned fibers confirmed the orientation of polymer chains, with PHBV chains preferentially oriented along the fiber axis. The degree of orientation increased with increasing fiber take-up velocity. X-ray diffraction pattern also indicates the development of β -form crystal in electrospun PHBV fibers collected at an angular velocity of 1500 rpm. The thermal behavior of electrospun PHBV fibers was studied using modulated differential scanning calorimetry. The tensile properties of single electrospun PHBV fibers were studied using a nanotensile tester. Our results indicate that electrospun PHBV fiber with a higher degree of molecular orientation exhibits a higher tensile modulus and strength but lower strain at break.

Introduction

Natural source poly(hydroxyalkanoates) (PHAs) are a class of biodegradable and biocompatible thermoplastic polyesters produced by numerous bacteria as intracellular carbon and energy storage materials.¹ They have been attractive for their promising environmental, pharmaceutical, and biomedical applications.^{2–4} To further improve their mechanical property for practical applications, many methods have been employed, including annealing,^{5–8} copolymerization,^{9,10} and blending.^{11,12} Among these methods, annealing is a practical and economical method, especially with PHA fibers. High strength melt spun poly[(R)-3-hydroxybutyrate-*co*-(R)-3-hydroxyvalerate] (PHBV) fibers with tensile strength over 1 GPa were prepared by one-step cold-drawing at room temperature, as reported recently by Tanaka et al.⁷ Their results suggested that the high tensile strength is due to the highly oriented molecular structure as well as the planar zigzag conformation formed through stretching PHBV chains in the amorphous region during cold-drawing. PHBV fibers with higher drawing ratio displayed higher tensile strength.

Electrospinning is an effective fiber fabrication technique which utilizes electrostatic forces to draw polymer solution or melt into fibers with diameters ranging from micro- to nanometer scale. A variety of electrospun polymer fibers have been successfully fabricated with potential applications in microelectronics, sensing, membrane-based separation, and tissue engineering.^{13–18} Macroscopically aligned electrospun fibers

have also been fabricated using a modified collector such as a counter electrode collector and a rotating collector.^{19–22} Similar to conventional cold-drawing on melt spun fibers, rotating collection is expected to provide additional drawing force to assist the orientation of polymer chains in their electrospun fibers. Molecular orientation in electrospun nylon 6 fibers collected onto a rotating collector has been studied.²⁰ At high windup speed, the substantial orientation of α -crystal and reduced γ -crystal content were ascribed to the stretching of nylon 6 chains during collection onto the rotating collector.

Only recently has mechanical characterization on single electrospun polymer fiber been carried out because of its small size. The axial modulus of single electrospun poly(L-lactide) (PLLA) fiber was measured by three-point bending test using an atomic force microscope.²³ To evaluate the ultimate tensile strength and tensile strain of single electrospun fiber, a nanotensile testing system has been developed.^{24–27} The tensile modulus and strength of single electrospun PLLA fiber collected on a rotating collector were investigated using a nanotensile tester.²⁴ The tensile property of single electrospun polyimide nanofiber was also investigated.²⁵ However, systematic study on the structure–mechanical property relationship of single electrospun polymer fiber is very limited.²⁶

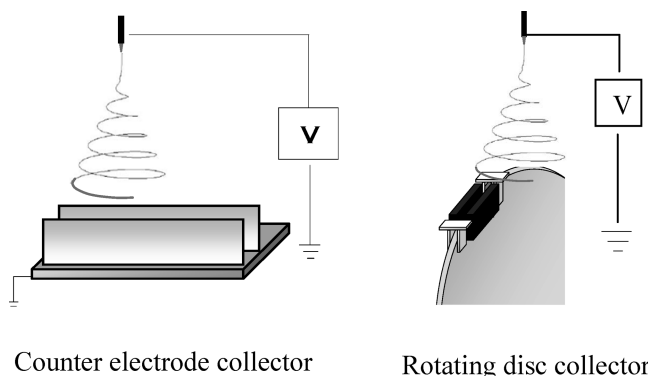
Electrospun PHA fibers have been successfully fabricated,^{28–33} and their applications as fibrous scaffolds for tissue engineering have also been investigated.^{31–33} One of the important prerequisites of electrospun fibrous scaffolds for tissue engineering is their mechanical compatibility with the target tissue, which determines cell adhesion, cell shape, and ultimately the cellular functions.^{34,35} However, to our knowledge, the tensile property of single electrospun PHA fiber and its relation to the molecular conformation of PHAs have not been systematically studied yet. Herein, we report our results on the molecular orientation and tensile property of single electrospun PHBV fiber fabricated by using different fiber collectors such as a counter electrode

* Corresponding authors. Phone: +65-6874-8421 (X.L.); +81-75-724-7323 (M.K.); +65-6874-8145 (C.B.H.). Fax +65-6872-7528 (X.L.); +81-75-724-7800 (M.K.); +65-6872-7528 (C.B.H.). E-mail: x-li@imre.a-star.edu.sg (X.L.); m-kotaki@kit.ac.jp (M.K.); cb-he@imre.a-star.edu.sg (C.B.H.).

[†] Kyoto Institute of Technology.

[‡] A*STAR (Agency for Science, Technology and Research).

[§] National University of Singapore.



Counter electrode collector

Rotating disc collector

Figure 1. Schematic diagrams for the counter electrode collector and modified rotating disk collector.

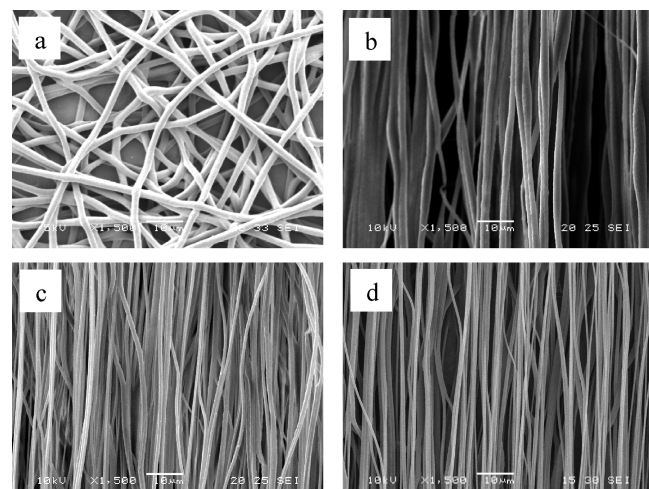
collector and a rotating disk collector. The internal structure of electrospun PHBV fibers was characterized using modulated differential scanning calorimetry (MDSC), polarized Fourier transform infrared (PFTIR) spectroscopy, and 2-D wide-angle X-ray diffraction (WAXD). The tensile property of single electrospun PHBV fiber was evaluated via nanotensile testing. Our results demonstrate that the mechanical property of single electrospun PHBV fiber is strongly influenced by its crystalline morphology and polymer chain conformation, which can be controlled by the electrospinning condition.

Experimental Section

Materials. Natural source poly[(*R*)-3-hydroxybutyrate-*co*-(*R*)-3-hydroxyvalerate] (PHBV) with hydroxyvalerate (HV) content of 8 wt % ($M_w = 600\,000$, $M_w/M_n = 3.7$) was purchased from Aldrich, and purified by dissolving in chloroform followed by filtration and subsequent precipitation in hexane. Chloroform and 1,2-dichloroethane were obtained from Aldrich and were used as received.

Electrospinning PHBV Fibers. PHBV solution for electrospinning was prepared by dissolving the purified PHBV in a mixed solvent of chloroform and 1,2-dichloroethane (2/3; W/W) at 12 wt %. The mixture was stirred at 50 °C overnight to ensure complete dissolution of PHBV. Electrospinning was carried out with the prepared PHBV solution at an applied voltage of 12 kV using a 22 gauge size needle (about 0.4 mm inner diameter opening) with a needle-to-collector distance of 150 mm. The flow rate of PHBV solution was set as 0.5 mL/h using a syringe pump. For this study, a grounded counter electrode collector or rotating disk collector was used to collect macroscopically aligned electrospun PHBV fibers. The counter electrode collector consists of two parallel aluminum electrodes with a gap distance of 25 mm. In order to collect single electrospun fiber for the tensile test, the disk collector was modified by fixing two aluminum electrodes placed parallel to each other with a gap distance of 25 mm. The schematic diagrams for the counter electrode collector and modified disk collector are shown in Figure 1. The electrospun fibers were deposited on the disk collector at various angular velocities of 750 and 1500 rpm or at an associated linear velocity of 470 and 940 m/min, respectively.

Characterization of Electrospun Fibers. The morphology of electrospun PHBV fibers was examined using a scanning electron microscope (SEM, JEOL JSM-5600). Fiber diameters had been measured using the software ImageJ. Modulated differential scanning calorimetry (MDSC) thermograms were obtained using a TA Instruments 2920 differential scanning calorimeter at modulated mode and equipped with an autocool

**Figure 2.** SEM micrographs of electrospun PHBV fibers collected with different collectors: stationary flat plate (a); counter electrode collector (b); rotating disk collector with an angular velocity of 750 rpm (c) and 1500 rpm (d), respectively.

accessory and calibrated using indium. The MDSC was operated under a nitrogen atmosphere at a heating rate of 2 °C/min from -30 to 200 °C with a modulation period of 60 s at an amplitude of ± 0.318 °C. Polarized Fourier transform infrared spectra were collected using a Bruker Equinox 55 Fourier transform infrared spectrometer with polarizing function; 32 scans were signal-averaged with a resolution of 2 cm⁻¹ at room temperature. In the parallel polarization, the direction of the electric vector of the incident beam is parallel to the fiber axis, while, in the perpendicular polarization, it is perpendicular to the fiber axis. Wide-angle X-ray diffraction (WAXD) measurements were carried out by using a Bruker GADDS diffractometer with an area detector operating under Cu K α (1.5418 Å) radiation (40 kV, 40 mA) at room temperature. Macroscopically aligned fiber mats deposited on a paper frame were mounted on a sample holder with double-sided adhesive tape.

Tensile Testing on Single Electrospun Fiber. PHBV fibers were first electrospun onto a collector in a short spinning time. With the use of a bright lamp light, the excessive fibers were carefully removed until a single straight fiber was left between the aluminum electrode gap. The single fiber is then mounted on a paper frame with a gauge length of 10 mm. The paper frame was subsequently mounted onto a Nanomechanical Testing System (Nano UTM, MTS Systems Corporation). Immediately prior to starting the tensile test, the vertical sides of the paper frame were cut off and the single specimen was then pulled at a constant strain rate of 1% per minute with 50 nN load resolution within a 500 mN load range. Five specimens prepared under the same processing conditions were tested for each tensile test. The fiber diameters were measured by SEM observation of the fiber segments not subjected to stress for calculation of tensile strength.

Results and Discussion

Electrospinning of PHBV Fibers. The morphologies of electrospun PHBV fibers prepared under the same electrospinning conditions but with different collectors were examined using scanning electron microscopy (SEM), and the images are shown in Figure 2. Due to bending instability of the charged jet, a randomly aligned fibrous mat was formed on the stationary flat plate (Figure 2a). On the other hand, macroscopically aligned fibers could be fabricated onto a counter electrode collector or

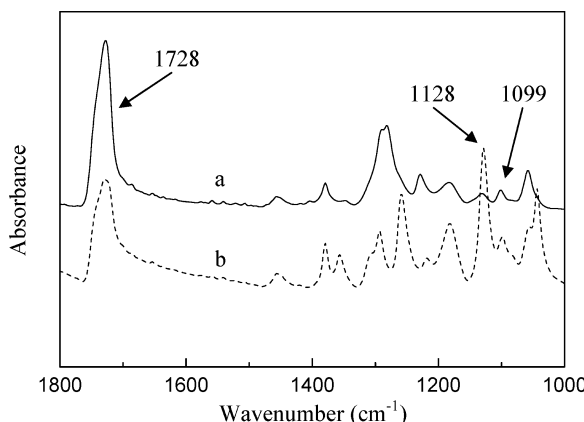


Figure 3. Polarized FTIR spectra of macroscopically aligned electrospun PHBV fibers collected on a rotating disk collector with an angular velocity of 1500 rpm: Electric vector of the incident IR beam perpendicular to the fiber axis (a) and parallel to the fiber axis (b), respectively.

rotating disk collector. In this study, the disk collector was operated at an angular velocity of 750 and 1500 rpm, or at an associated linear velocity of 470 and 940 m/min, respectively. The average fiber diameter was found to be 1752 ± 179 nm for fibers collected using a stationary flat plate and 1680 ± 112 nm for those collected using a counter electrode collector. The negligible change in fiber diameter suggests counter electrode collection did not impose additional mechanical drawing force onto electrospun PHBV fibers. A similar observation has been reported with macroscopically aligned electrospun poly(ethylene oxide) (PEO) fibers collected using a counter electrode collector.¹⁹ In contrast, the average diameter for fibers collected with a rotating disk collector was reduced to 728 ± 98 and 513 ± 75 nm at an angular velocity of 750 and 1500 rpm, respectively. Observed reduction in fiber diameter indicates the existence of an additional mechanical drawing force imposed on the electrospun PHBV fibers. The thinner PHBV fiber at an angular velocity of 1500 rpm could be attributed to the stronger drawing force. It is clear that, under rotating disk collection, the electrospun PHBV fibers were further stretched and aligned toward the roll up direction.

Molecular Orientation of Electrospun PHBV Fibers. To understand the influence of the electrospinning process and fiber collection on the orientation of PHBV chains, macroscopically aligned electrospun PHBV fibers collected under various conditions were studied using Fourier transform infrared spectroscopy, differential scanning calorimetry, and 2-D wide-angle X-ray diffraction.

Polarized Fourier transform infrared spectroscopy (PFTIR) has been widely used in investigating the conformational changes of polymer chains during electrospinning.^{19,20,36} For FTIR spectra characterized by polarized infrared radiation, a high absorbance intensity can be measured if the bonding direction coincides with the electric vector of the incident IR beam. To study the molecular orientation of PHBV chains in the macroscopically aligned fibers, electrospun PHBV fibers collected with a pair of counter parallel electrodes or a rotating disk collector were characterized using PFTIR. Figure 3 shows the parallel and perpendicular PFTIR spectra of aligned PHBV fibers collected on a rotating disk collector with an angular velocity of 1500 rpm as a typical example. As shown in Figure 3, PFTIR spectra for the aligned fibers in two mutually perpendicular directions exhibit a clear difference in absorbance intensity. This indicates the presence of molecular orientation of PHBV chains

TABLE 1: Dichroic Ratio (*R*) of Different Vibrational Bands of Aligned PHBV Fibers

| vibration band (cm ⁻¹) | angular velocity (rpm) | | |
|------------------------------------|------------------------|-------|-------|
| | 0 ^a | 750 | 1500 |
| 1099 (symmetric C—O stretching) | 2.15 | 4.02 | 6.54 |
| 1128 (asymmetric C—O stretching) | 3.64 | 10.25 | 14.21 |
| 1728 (C=O stretching) | 0.83 | 0.73 | 0.64 |

^a 0 refers to fibers collected with a counter electrode collector.

in the aligned fibers. To characterize molecular orientation quantitatively, dichroic ratio (*R*) is calculated by the equation $R = A_{||}/A_{\perp}$, where $A_{||}$ is the parallel-polarized infrared absorbance intensity and A_{\perp} is the perpendicular-polarized infrared absorbance intensity for a particular vibration. For a randomly oriented sample, *R* is equal to 1, while, for an anisotropic sample with polymer chains oriented along the fiber axis, *R* is equal to infinity. As listed in Table 1, the *R* for carbonyl stretching (C=O; ~ 1728 cm⁻¹) is calculated as 0.83, 0.73, and 0.64 for macroscopically aligned PHBV fibers collected with a counter electrode collector and a rotating disk collector at an angular velocity of 750 and 1500 rpm, respectively. $R < 1$ indicates that the absorbance intensity of C=O is lower when the electric vector of the incident infrared beam is parallel to the fiber axis, in comparison to the case when the vector is perpendicular to the fiber axis. This suggests that the carbonyl bond exhibits perpendicular polarization to the fiber axis, and PHBV chains are oriented along the fiber axis because the carbonyl bond is perpendicular to the PHBV backbone as anticipated from its molecular structure. On the other hand, higher *R* values for the asymmetric and symmetric stretching of the C—O—C bond along the PHBV backbone suggest they are in parallel polarization to the fiber axis. Study showed that the *R* for the symmetric C—O—C stretching and asymmetric C—O—C stretching increases from 2.15 to 6.54 and from 3.64 to 14.21 with increasing angular velocity from 0 to 1500 rpm, respectively. This suggests that, at higher angular velocity, stronger drawing force leads to better orientation of PHBV chains along the fiber axis. The decrease of *R* for C=O from 0.83 to 0.64 with increasing angular velocity from 0 to 1500 rpm also indicates a higher degree of molecule orientation at higher angular velocity.

Carbonyl stretching in PHAs has a strong correlation to PHA conformation because the C—H \cdots O hydrogen bonding between the C=O group and CH₃ group has shown the capability to stabilize a particular molecular conformation.^{37,38} Figure 4 shows the expansion of the carbonyl stretching region of conventional (unpolarized) FTIR spectra for as-received PHBV and aligned PHBV fibers. The carbonyl stretching band of as-received PHBV can be resolved into an intensive band at 1723 cm⁻¹ and a weak shoulder at 1740 cm⁻¹, as shown in Figure 4d, corresponding to the carbonyl stretching band of crystalline PHBV and amorphous PHBV, respectively.³⁷ In comparison to the spectrum of as-received PHBV, spectra of aligned PHBV fibers show an additional peak at 1732 cm⁻¹ and its relative intensity increases with increasing angular velocity. An additional peak at 1732 cm⁻¹ has been reported in the crystallization of poly[(R)-3-hydroxybutyrate] (PHB) previously, and it was assigned to the intermediate phase between the PHB amorphous phase and the crystalline phase.³⁹ Here, this additional peak could be assigned to oriented amorphous PHBV chains. The observation of an additional peak at 1732 cm⁻¹ with aligned PHBV fibers collected using a counter electrode collector suggests that the drawing force provided during electrospinning is strong enough to orient PHBV chains in the

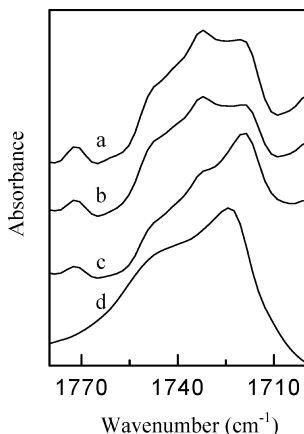


Figure 4. FTIR spectra of macroscopically aligned electrospun PHBV fibers and as-received PHBV: rotating disk collecting at 1500 rpm (a) and 750 rpm (b), respectively; counter electrode collecting (c) and as-received PHBV (d).

amorphous phase. The increase in intensity of carbonyl stretching at 1732 cm^{-1} with increasing angular velocity is attributed to a higher degree of PHBV chain orientation in the amorphous phase. The shift of the carbonyl stretching band of crystalline PHBV at 1723 cm^{-1} for as-received PHBV to 1718 cm^{-1} for aligned PHBV fibers is possible due to a closer crystalline packing in electrospun PHBV fiber.³⁷

The orientation of PHBV chains in its macroscopically aligned fibers was further investigated by 2-D wide-angle X-ray diffraction (WAXD). Figure 5 shows the 2-D WAXD patterns of as-received PHBV and aligned PHBV fibers collected with a rotating disk collector at an angular velocity of 750 and 1500 rpm, respectively. The patterns for aligned fibers were obtained with the *c*-axis parallel to the fiber axis. The bright rings in the 2-D WAXD pattern for as-received PHBV suggest a random distribution of crystallographic planes in as-received PHBV. On the other hand, bright arcs along the equators of the patterns for aligned PHBV fibers (as shown in Figure 5b and c) suggest the existence of crystallographic planes located parallel to the fiber axis of aligned fibers. In comparison to the 2-D patterns of as-received PHBV or aligned PHBV fibers collected at 750 rpm, two additional arcs are observed in the 2-D pattern of PHBV fibers collected at 1500 rpm, as shown in Figure 5c. These additional arcs could be assigned to the β -form crystal of PHBV, similar to a previous report on cold drawn PHB fiber.⁴⁰ It is well established that PHBV crystal has fold chain crystal (FCC) or α -form crystal with molecules in 2/1 helix conformation and extended chain crystal (ECC) with amorphous PHBV molecules in planar zigzag conformation (β -form crystal), tied between PHBV crystallites. Formation of β -form crystal is due to the orientation of PHBV molecules in the amorphous region between lamellar crystallites under stretching.

Figure 6 shows the radial average intensity plotted against azimuthal angle (χ) for the reflection at (020) of aligned PHBV fibers. A fairly sharp peak at $\chi = -90^\circ$ (equator) is observed for the fibers collected at an angular velocity of 1500 rpm, whereas, for the fibers collected at 750 rpm, the peak appears tilted away from this angle. This indicates that the crystals within PHBV fibers collected at 1500 rpm are orientated more closely to the fiber axis due to the stronger drawing force. The full width at half-maximum (fwhm) of the plot indicated a value of 25.9 for fibers electrospun at 1500 rpm and 37.5 for 750 rpm, respectively. Improved crystallite orientation in the direction of the fiber axis is represented by a narrower fwhm. A similar

trend in crystallite orientation has been observed with melt spun PHB fibers performed one step drawing, as reported by Tanaka et al.⁴⁰

To quantify the degree of orientation of the crystallite axis in the electrospun fibers, Herman's orientation function (f) was applied. The value of f is 1 when the polymer chains aligned perfectly parallel to the fiber axis and -0.5 when the polymer chains aligned perfectly perpendicular to the fiber axis. When f is zero, it means the random orientation of the chains. In our case, the calculation of f was simplified by simply calculating the misorientation appearing in the azimuthal scan by the following equation:

$$f = \frac{180^\circ - \Delta\varphi_{1/2}}{180^\circ} \quad (1)$$

where $\Delta\varphi_{1/2}$ represents the fwhm of the azimuthally scanned peak. f is calculated as 0.79 and 0.86 for fibers collected at an angular velocity of 750 and 1500 rpm, respectively. It is clear that f increases with increasing angular velocity, indicating the crystals in the fibers are oriented along the fiber axis and the degree of crystal orientation increases as the angular velocity is increased. Moreover, the high value of f ($f = 0.86$, which is close to 1) with the fibers collected at an angular velocity of 1500 rpm indicates the ECC structure is dominant in the fibers, as discussed above. Therefore, as demonstrated by the PFTIR and WAXD results, it is clear that PHBV fibers collected at an angular velocity of 1500 rpm exhibits dominant ECC structure with amorphous PHBV chains in a planar zigzag conformation, while the fibers collected at an angular velocity of 750 rpm or using a counter electrode collector exhibit FCC structure with various degrees of orientation of amorphous PHBV chains.

The thermal behaviors of as-received PHBV and electrospun PHBV fibers were investigated using temperature modulated differential scanning calorimetry (MDSC), and their thermograms are shown in Figure 7. In addition, the numerical values corresponding to thermal transition are listed in Table 2. As shown in Figure 7a, the broad and strong endothermal transition centered at $160.6\text{ }^\circ\text{C}$ with an enthalpy of 74.4 J/g is the melting transition of recrystallized α -form PHBV crystallite. The broad endothermal transition suggests a wide distribution of PHBV crystallite sizes, and the shoulder peak observed at $145.5\text{ }^\circ\text{C}$ is attributed to α -form PHBV crystallite in small size. In contrast, the endothermal peaks of electrospun PHBV fibers are narrowed and shifted to higher temperature with the absence of endothermal shoulder for electrospun fibers collected using a counter electrode collector or rotating disk collector at an angular velocity of 750 rpm. All of these indicate the orientation of PHBV chains in the electrospun fibers could lead to more uniform PHBV crystallite. The shoulder peak observed at $150.0\text{ }^\circ\text{C}$ ($4.5\text{ }^\circ\text{C}$ higher than that of as-received PHBV) in the thermogram of electrospun PHBV fibers collected at an angular velocity of 1500 rpm is the melting transition of PHBV crystallite with dominant ECC structure. The relatively lower melting transition temperature of the recrystallized PHBV crystallite in the fibers collected at 1500 rpm, in comparison to those of other electrospun PHBV fibers, is possible due to the influence of the planar zigzag conformation on the recrystallization of PHBV crystallite.

MDSC superimposes a low frequency amplitude temperature onto a linear heating ramp of standard DSC. By using MDSC, one can separate total heat flow into a heat capacity-related (reversing) component and a time dependent nonreversing component. As for the thermal events associated with nonre-

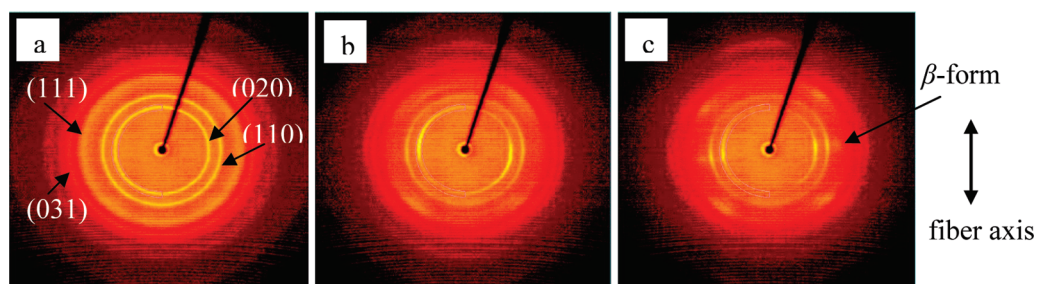


Figure 5. XRD patterns of PHBV cast film and macroscopically aligned electrospun PHBV fibers collected using a rotating disk collector at various angular velocities: PHBV cast film (a); rotating disk collecting at an angular velocity of 750 rpm (b) and 1500 rpm (c), respectively.

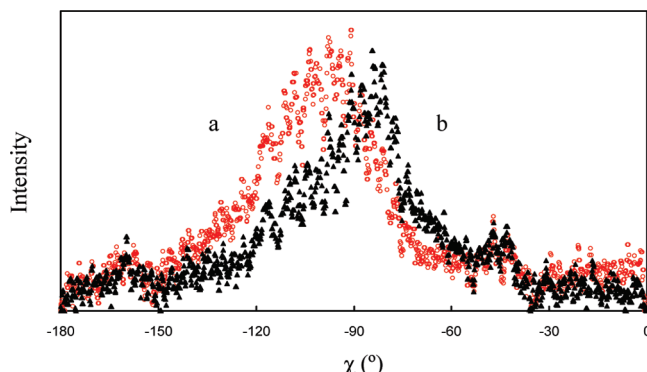


Figure 6. Radial average intensity versus azimuthal angle plot obtained from 2-D WAXD for the (020) reflection of aligned electrospun PHBV fibers collected with an angular velocity of 750 (a) and 1500 rpm (b), respectively.

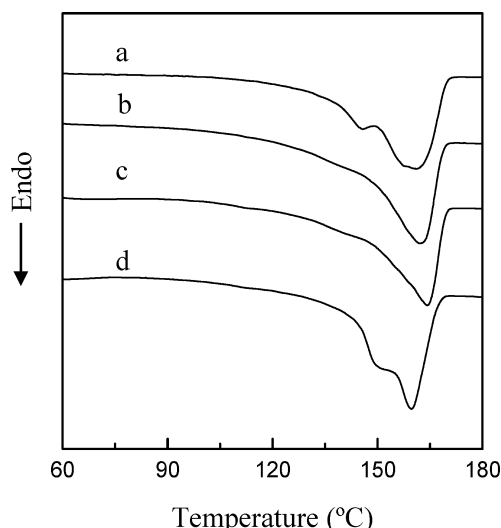


Figure 7. MDSC curves in total heat flow for as-received PHBV and aligned electrospun PHBV fibers: as-received PHBV (a); counter electrode collecting (b); rotating disk collecting at 750 rpm (c) and 1500 rpm (d), respectively.

versing heat flows, they are usually caused by responses which are not in phase with the temperature oscillations. Gunaratne et al.⁴¹ had previously studied the melting behavior of PHB with different thermal histories. The authors had found that PHB which has undergone slow cooling processes has the lowest reversing melting contribution, and had stated that poorly crystallized polymers have larger endothermic reversing contributions and smaller endothermic nonreversing contributions compared to stable and perfect crystals. Calculating the contribution of reversing heat flow to the total heat flow based on Table 2, the contribution for as-received PHBV, electrospun fibers collected with a stationary collector, a rotating disk

TABLE 2: Thermal Property Results of As-Received PHBV and Its Electrospun Fibers Studied Using MDSC

| | as-received PHBV | electrospun PHBV fiber | | |
|---------------------------|---------------------------|------------------------|------------------|-------------------------|
| | | 0 ^a | 750 ^b | 1500 ^b |
| $\Delta H_{m,R}^c$ (J/g) | 43.7 | 25.1 | 23.6 | 21.8 |
| $\Delta H_{m,NR}^d$ (J/g) | 30.7 | 43.5 | 41.7 | 46.4 |
| T_m^e (°C) | 160.6(145.5) ^f | 162.3 | 164.4 | 160.0(150) ^f |

^a 0 refers to fibers collected with a counter electrode collector.

^b Electrospun fibers collected using a rotating disk collector with an angular velocity of 750 and 1500 rpm, respectively. ^c Melting enthalpy measured in reversing heat flow. ^d Melting enthalpy measured in nonreversing heat flow. ^e Peak maximum of melting transition measured in total heat flow. ^f Peak maximum of shoulder melting transition measured in total heat flow.

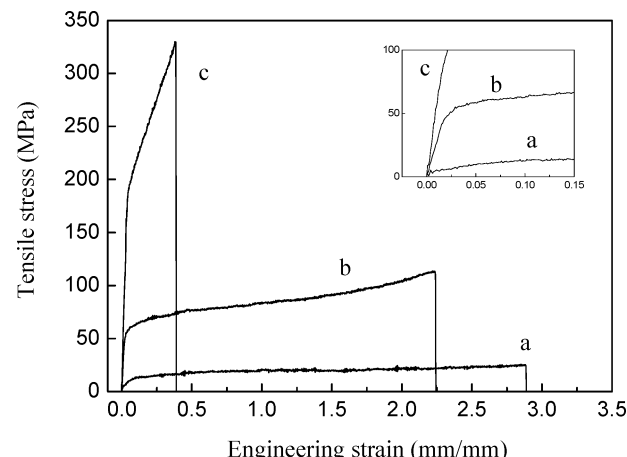


Figure 8. Representative stress-strain curves for single electrospun PHBV fiber collected using different collectors: counter electrode collector (a); rotating disk collector with an angular velocity of 750 rpm (b) and 1500 rpm (c), respectively. (The inset shows the enlarged portion of the stress-strain curve at the low strain regime.)

collector at 750 and 1500 rpm are 0.59, 0.37, 0.36, and 0.30, respectively. This observation suggests that electrospun fibers may be composed of relatively stable crystal structures, and this suggestion is reasonable, considering that tensile strength was applied to stretch the molecular chains. Moreover, since extended chain crystals have been found as being related to nonreversing heat flow as observed in PEO,⁴² it may be acceptable to consider the higher proportion of nonreversing heat flow to the presence of extended chain crystals within electrospun fibers collected at 1500 rpm.

Tensile Property of Single Electrospun PHBV Fiber. Mechanical properties of single electrospun PHBV fiber had been evaluated using a nanotensile tester. Figure 8 shows the representative stress-strain curves for the PHBV fibers collected using a counter electrode collector and rotating disk collector at an angular velocity of 750 and 1500 rpm, respectively; the

TABLE 3: Tensile Properties of Single Electrospun PHBV Fibers

| angular velocity (rpm) | tensile modulus (GPa) | tensile strength (MPa) | strain at break (mm/mm) |
|------------------------|-----------------------|------------------------|-------------------------|
| 0 ^a | 0.15 ± 0.05 | 22.91 ± 5.81 | 2.83 ± 0.23 |
| 750 | 1.22 ± 0.55 | 81.97 ± 31.78 | 2.51 ± 0.19 |
| 1500 | 2.67 ± 0.94 | 268.01 ± 52.22 | 0.57 ± 0.24 |

^a 0 refers to fibers collected with a counter electrode collector.

numerical values are summarized in Table 3. It can be seen that both tensile modulus and tensile strength increase with increasing angular velocity, and the highest average tensile modulus and strength were found with the electrospun PHBV fiber collected with a rotating disk collector at an angular velocity of 1500 rpm. As shown in Figure 8c, two nearly linear stress-strain stages are observed in its stress-strain curve. While the first stage could be described as the linearly elastic deformation region, the second stage corresponds to the linearly strain-hardening region with larger plastic deformation until the final breakage. The stress and strain for transition from elastic deformation region to strain-hardening region were determined as 190.32 ± 38.75 MPa and 0.05 ± 0.02 , respectively. These indicate that the electrospun PHBV fibers collected at an angular velocity of 1500 rpm exhibit strain-hardening ductile behavior, a clear indication that the fibers were prestretched by the rotating collector. In contrast, a long plateau stage was observed after linear elastic deformation in the stress-strain curve of the PHBV fiber collected at 750 rpm (Figure 8b). The average tensile modulus and strength were measured at a relatively lower value of 1.22 ± 0.55 GPa and 81.97 ± 31.78 MPa, respectively. Furthermore, the initial plateau was observed at a much lower stress of 59.34 ± 21.58 MPa. Similar tensile behavior was also observed for PHBV fibers collected using a counter electrode collector, as shown in Figure 8a. However, their tensile modulus and strength are much lower than those fibers collected using a rotating disk collector. The enlarged portion of stress-strain curves at the low strain regime as shown in the inset of Figure 8 clearly demonstrates the modulus difference between the PHBV fibers collected under different conditions.

The measured tensile properties of single electrospun PHBV fiber can be correlated to the molecular conformation of PHBV chain in its fiber. Electrospun PHBV fiber collected at an angular velocity of 1500 rpm exhibits aligned lamellae and fibrillar structures or ECC structure, as indicated by its FTIR, WAXD, and DSC results. Its amorphous regions most likely consist of extended PHBV chains in a planar zigzag conformation. Such a high degree of molecular orientation in the direction of the fiber axis is expected to result in a higher axial tensile modulus and strength with lower strain (Figure 8c). On the other hand, PHBV fiber collected at 750 rpm exhibits a less aligned lamellae structure and the PHBV chains in amorphous regions are most likely in an entangled state. Under external tensile force, such lamellae structure would produce less resistance and the entangled PHBV chains would disentangle, leading to high elongation at break and observation of long plateau in its stress-strain curve (Figure 8b). The low tensile modulus and strength of PHBV fiber (Figure 8a) collected using a counter electrode collector could be explained by its lower molecular orientation in comparison to those fibers collected using a rotating disk collector as observed in FTIR, WAXD, and DSC study.

Conclusions

Macroscopically aligned electrospun PHBV fibers have been successfully fabricated through electrospinning using a counter

electrode collector or a rotating disk collector. The molecular conformation of PHBV in the prepared fibers has been studied using PFTIR, MDSC, and WAXD. The dichroic ratios calculated from PFTIR spectra of electrospun PHBV fibers indicate that the electrostatic force imposed during electrospinning can orient PHBV molecular chains along the direction of the fiber axis, and rotating disk collection provides additional drawing force to assist the orientation of PHBV chains and the degree of orientation is increased with increasing angular velocity. WAXD study demonstrates that crystallographic planes are oriented along the fiber axis in the fibers collected with a rotating disk collector and β -form crystal is developed in electrospun PHBV fibers collected at an angular velocity of 1500 rpm. MDSC results also suggest the existence of oriented PHBV molecular chains in electrospun PHBV fibers.

Tensile properties of single electrospun PHBV fiber have been investigated using a nanotensile tester. The highest tensile modulus and strength were observed with PHBV fibers collected with a rotating disk collector at an angular velocity of 1500 rpm. This characteristic is attributed to its high degree of molecular orientation, which was induced by the large drawing force provided by the rotating disk collector. Larger drawing force could result in aligned lamellae and fibrillar structure in the fibers with the amorphous regions consisting of extended PHBV molecular chains in planar zigzag conformation, showing strong resistance to the axial tensile force. On the other hand, at lower angular velocity or collecting with counter electrode collector, the degree of molecular orientation is lower and the obtained PHBV fibers exhibited a lower tensile modulus and strength with observation of a plateau in their stress-strain curves. Therefore, our results demonstrate the mechanical property of single electrospun PHBV fiber could be tailored by manipulating the molecular orientation of PHBV chains through changing the fiber collection method and conditions, to match different requirements.

References and Notes

- (1) Doi, Y. *Microbial Polyester*; VCH Publisher: New York, 1990.
- (2) Lenz, R. W.; Marchessault, R. H. *Biomacromolecules* **2005**, *6*, 1–8.
- (3) Chen, G. Q.; Wu, Q. *Biomaterials* **2005**, *26*, 6565–6578.
- (4) Dai, Z. W.; Zou, H. X.; Chen, G. Q. *Biomaterials* **2009**, *30*, 3075–3083.
- (5) de Koning, G. J. M.; Scheeren, A. H. C.; Lemstra, P. J.; Peeters, M.; Reynaers, H. *Polymer* **1994**, *35*, 4598–4605.
- (6) Hobbs, J. K.; Barham, P. J. *J. Mater. Sci.* **1998**, *33*, 2515–2518.
- (7) Tanaka, T.; Fujita, M.; Takeuchi, A.; Suzuki, Y.; Uesugi, K.; Ito, K.; Fujisawa, T.; Doi, Y.; Iwata, T. *Macromolecules* **2006**, *39*, 2940–2946.
- (8) Furuhashi, Y.; Imamura, Y.; Jikihara, Y.; Yamane, H. *Polymer* **2004**, *45*, 5703–5712.
- (9) Andrade, A. P.; Witholt, B.; Chang, D. L.; Li, Z. *Macromolecules* **2003**, *36*, 9830–9835.
- (10) Li, X.; Loh, X. J.; Wang, K.; He, C. B.; Li, J. *Biomacromolecules* **2005**, *6*, 2740–2749.
- (11) Li, X.; Liu, K. L.; Wang, M.; Wong, S. Y.; Tjiu, W. C.; He, C. B.; Goh, S. H.; Li, J. *Acta Biomater.* **2009**, *5*, 2002–2012.
- (12) Scandola, M.; Focarete, M. L.; Adamus, G.; Sikoska, W.; Baranowska, I.; Swierczek, S.; Gnatowski, M.; Kowalcuk, M.; Jedlinski, Z. *Macromolecules* **1997**, *30*, 2568–2574.
- (13) Peng, H. S.; Zhou, S. B.; Jiang, J.; Guo, T.; Zheng, X. T.; Yu, X. J. *J. Phys. Chem. B* **2009**, *113*, 4636–4641.
- (14) Greiner, A.; Wendorff, J. H. *Angew. Chem., Int. Ed.* **2007**, *46*, 5670–5703.
- (15) Wang, G.; Ji, Y.; Huang, X. R.; Yang, X. Q.; Gouma, P. I. *J. Phys. Chem. B* **2006**, *110*, 23777–23782.
- (16) Hong, Y. L.; Fan, H. S.; Zhang, X. D. *J. Phys. Chem. B* **2009**, *113*, 5837–5842.
- (17) Zhang, Y. Z.; Su, B.; Ramakrishna, S.; Lim, C. T. *Biomacromolecules* **2008**, *9*, 136–141.
- (18) Blond, D.; Walshe, W.; Young, K.; Blighe, F. M.; Khan, U.; Almecija, D.; Carpenter, L.; McCauley, J.; Blau, W. J.; Coleman, J. N. *Adv. Funct. Mater.* **2008**, *18*, 2618–2624.

- (19) Kakade, M. V.; Givens, S.; Gardner, K.; Lee, K. H.; Chase, D. B.; Rabolt, J. F. *J. Am. Chem. Soc.* **2007**, *129*, 2777–2782.
- (20) Lee, K. H.; Kim, K. W.; Pesapane, A.; Kim, H. Y.; Rabolt, J. F. *Macromolecules* **2008**, *41*, 1494–1498.
- (21) Chew, S. Y.; Mi, R.; Hoke, A.; Leong, K. W. *Biomaterials* **2008**, *29*, 653–661.
- (22) Chew, S. Y.; Mi, R.; Hoke, A.; Leong, K. W. *Adv. Funct. Mater.* **2007**, *17*, 1288–1296.
- (23) Tan, E. P. S.; Lim, C. T. *Nanotechnology* **2006**, *17*, 2649–2654.
- (24) Inai, R.; Kotaki, M.; Ramakrishna, S. *Nanotechnology* **2005**, *16*, 208–213.
- (25) Chen, F.; Peng, X. W.; Li, T. T.; Chen, S. L.; Wu, X. F.; Reneker, D. H.; Hou, H. Q. *J. Phys. D: Appl. Phys.* **2008**, *41*, 025308.
- (26) Lim, C. T.; Tan, E. P. S.; Ng, S. Y. *Appl. Phys. Lett.* **2008**, *92*, 141908.
- (27) Chew, S. Y.; Hufnagal, T. C.; Lim, C. T.; Leong, K. W. *Nanotechnology* **2006**, *17*, 3880–3891.
- (28) Ying, T. H.; Ishii, D.; Mahara, A.; Murakami, S.; Yamaoka, T.; Sudesh, K.; Samian, R.; Maeda, M.; Iwata, T. *Biomaterials* **2008**, *29*, 1307–1317.
- (29) Meng, W.; Kim, S. Y.; Yuan, J.; Kim, J. C.; Kwon, O. H.; Kawazoe, N.; Chen, G. P.; Ito, Y.; Kang, I. K. *J. Biomater. Sci., Polym. Ed.* **2007**, *18*, 81–94.
- (30) Ishii, D.; Lee, W. K.; Kasuya, K. I.; Iwata, T. *J. Biotechnol.* **2007**, *132*, 318–324.
- (31) Sombatmankhong, K.; Sanchavanakit, N.; Pavasant, P.; Supaphol, P. *Polymer* **2007**, *48*, 1419–1427.
- (32) Liang, D. H.; Hsiao, B. S.; Chu, B. *Adv. Drug Delivery Rev.* **2007**, *59*, 1392–1412.
- (33) Ndreu, A.; Nikkola, L.; Ylikuppila, H.; Ashammakhi, N.; Hasirci, V. *Nanomedicine* **2008**, *3*, 45–60.
- (34) Courtney, T.; Sacks, M. S.; Stankus, J.; Guan, J. J.; Wagner, W. R. *Biomaterials* **2006**, *27*, 3631–3638.
- (35) Lee, S. J.; Oh, S. H.; Liu, J.; Soker, S.; Atala, A.; Yoo, J. J. *Biomaterials* **2008**, *29*, 1422–1430.
- (36) Liu, Y.; Cui, L.; Guan, F.; Gao, Y.; Hedin, N. E.; Zhu, L.; Fong, H. *Macromolecules* **2007**, *40*, 6283–6290.
- (37) Sato, H.; Murakami, R.; Padermshoke, A.; Hirose, F.; Senda, K.; Noda, I.; Ozaki, Y. *Macromolecules* **2004**, *37*, 7203–7213.
- (38) Hu, Y.; Zhang, J.; Sato, H.; Futami, Y.; Noda, I.; Ozaki, Y. *Macromolecules* **2006**, *39*, 3841–3847.
- (39) Zhang, J.; Sato, H.; Noda, I.; Ozaki, Y. *Macromolecules* **2005**, *38*, 4274–4281.
- (40) Tanaka, T.; Yabe, T.; Teramachi, S.; Iwata, T. *Polym. Degrad. Stab.* **2007**, *92*, 1016–1024.
- (41) Gunaratne, L.M.W.K; Shanks, R. A. *J. Polym. Sci., Part B: Polym. Phys.* **2006**, *44*, 70–78.
- (42) Wunderlich, B.; Okazaki, I.; Ishikiriyama, K.; Boller, A. *Thermochim. Acta* **1998**, *324*, 77–85.

JP905820H